International Journal for Uncertainty Quantification, 5 (6): 545–568 (2015)

OPTIMAL SENSOR PLACEMENT FOR THE ESTIMATION OF TURBULENCE MODEL PARAMETERS IN CFD

Dimitrios I. Papadimitriou & Costas Papadimitriou*

Department of Mechanical Engineering, University of Thessaly, Pedion Areos 38334, Volos, Greece

*Address all correspondence to Costas Papadimitriou E-mail: costasp@uth.gr

Original Manuscript Submitted: 08/23/2015; Final Draft Received: 10/08/2015

The optimal placement of sensors for the estimation of turbulence model parameters in computational fluid dynamics is presented. The information entropy (IE), applied on the posterior uncertainty of the model parameters inferred from Bayesian analysis, is used as a scalar measure of uncertainty. Using an asymptotic approximation, the IE depends on nominal values of the CFD model and prediction error model parameters. It is derived from the sensitivities of the flow quantities predicted by the flow model with respect to the model parameters. A stochastic optimization algorithm is used to perform the minimization of the IE in the continuous design space. Robustness to uncertainties in the nominal model parameters and flow conditions is addressed. Information redundancy due to sensor clustering is addressed by introducing spatially correlated prediction error models. The algorithm is applied to the turbulent flow through a backward-facing step where the optimal locations of velocity and Reynolds shear stress profiles of sensors are sought for the estimation of the parameters of the Spalart-Allmaras turbulence model.

KEY WORDS: *Bayesian inference, information entropy, robustness, turbulence models*

1. INTRODUCTION

Uncertainty quantification methods for the estimation of the parameters of computational models based on experimental measurements have widely been developed in the engineering sciences. The uncertainties are usually quantified using probabilistic models, and the Bayesian inference framework is often used to combine information from computational tools and experimental data [1]. Among others, the Bayesian methodology has been applied to the identification of model parameters in structural dynamics [2–5], molecular dynamics [6–8], heat conduction [9], flight dynamics [10], and bioengineering [11]. The Bayesian approach has also been used to estimate the parameter of turbulence models for CFD computations [12–18].

The uncertainty in the estimation of the model parameters are due to mathematical model limitations as well as measurement errors and insufficiency of experimental data. The amount and quality of information that can be extracted from experimental data to infer the model parameter values depend on the number and type of sensors used and their location on the domain space. Optimal sensor placement (OSP) methodologies aim at defining the best locations of where to place the sensors so that the obtained experimental data are most informative for the estimation of the model parameters.

The optimization of sensor configurations for the identification of structural model parameters is been presented in [19, 20] based on information theory. The Fisher information matrix (FIM) [21], which is expressed by the sensitivities of the output quantities of interest (QoI) with respect to the parameters to be identified, has been introduced to quantify the performance of a chosen sensor configuration. The trace or the largest eigenvalue of the inverse of the FIM have been used as a performance measure. In [22, 23], it has been indicated that the determinant of the FIM, arising from

2152–5080/15/$35.00

the information entropy (IE), provides a rational measure of the amount of available information. The OSP was based on nominal values of the model parameters and prediction errors in order to compute the FIM or the IE. To account for the uncertainties in these nominal values, a robust IE index was introduced [22, 24]. The IE concept was also used to choose the optimal sensor locations for damage identification [25], for identification of nonlinear structural models [26, 27], water supply networks [28], and time-dependent problems such as wind flows around buildings based on a model falsification approach [29].

Most OSP studies dealt with design variables defined in discrete space. An exhaustive search of the optimal sensor configuration is computationally prohibitive. The minimization of the information entropy was performed using either stochastic optimization algorithms, such as genetic algorithms to explore an infinitesimal fraction of the total number of possible sensor configurations [30–32], or computationally very fast heuristic forward and backward sequential sensor placement algorithms [23, 33, 34] and hierarchical sensor placement strategies [29]. However, in a number of engineering fields, such as computational structural dynamics and CFD, the domains encountered are continuous and the sensor placement problem is formulated as an optimization over a continuous design space. Sensor clustering problems [35, 36] may then arise due to the fact that existing formulations do not preclude the selection of infinitesimally close neighbor sensors in a continuous space that provide exactly the same information. To avoid redundancy of information between sensors, Papadimitriou and Lombaert [35] used spatially correlated prediction error models to limit sensor clustering for structural dynamics applications, Stephan [37] used the closeness of FIM provided by two sensors for modal identification applications, while Papadopoulou et al. [29] used the joint entropy to incorporate spatial distribution of modeling errors in applications related to wind flows around buildings.

The optimal sensor location problem for model parameter estimation in CFD problems has not been widely examined yet. Relevant works include wind flows around buildings [29, 33] with the aim of optimal sensor location to improve the accuracy of predictions at unmeasured locations. A sensor placement approach for the estimation of unknown parameters of a distributed parameter system is applied to the case of chemical reaction in a tubular reactor [38], proving that the measurement location plays an essential role in the parameter estimation procedure. Also, in [39], different algorithms for optimal sensor location for the estimation of parameters in distributed systems are compared, and in [40], a technique for estimating aerodynamic parameters in real time from flight data is presented.

Bayesian formulations for the estimation of turbulence model parameters in CFD based on experimental data has been presented in [12–17] using Markov-chain Monte Carlo (MCMC) techniques [41–44] and in Papadimitriou and Papadimitriou [18] using asymptotic approximations. However, the optimal location of the sensors so that the resulting measurements are most informative for the estimation of the turbulence model or other parameters in CFD simulations has not been presented in the literature. The aim of the present work is to fill this gap and demonstrate the value of optimizing the sensor configuration.

Following previous developments, a Bayesian inference is used to quantify the posterior uncertainty in the model parameters of a CFD model given a sensor configuration. The information entropy, used as a measure of uncertainty in the parameters to be inferred using experimental data, is expressed asymptotically in terms of the derivatives with respect to the model parameters of the flow quantities predicted by the model at the location of sensors. The derivatives are computed using the direct differentiation of the flow model [45, 46]. A robust information entropy measure is introduced to design optimal sensor locations that are robust to uncertainties in the nominal model parameter values as well, as uncertainties in the flow conditions (e.g., Mach number, angle of attach, Reynolds number) under which the experiments are likely to be carried out. These uncertainties are quantified by the prior distributions postulated in the Bayesian formulation. The optimal sensor configuration is selected as the one that minimizes the robust information entropy. Thus the optimal sensor placement problem is formulated as an optimization problem with continuous design parameters associated with the location of sensors in the flow domain. Relying on a space discretization scheme to carry out the flow simulations, an interpolation scheme is used to compute the required information entropy values in locations different than the grid points in the mesh. To avoid the sensor clustering observed in optimal sensor placement problems applied on continuous design domains, a correlation structure of the prediction error model is introduced.

The proposed framework is generic and can be used for the parameter estimation for any CFD model. Emphasis, however, is laid on the estimation of turbulence model parameters, which pose the highest uncertainties compared

to other model parameters in CFD problems. The application is thus concerned with the estimation of the Spalart-Allmaras one-equation turbulence model parameters.

The presentation is organized as follows. In Section 2, the optimal sensor placement framework is presented. The CFD model equations and the direct differentiation approach for the computation of the required sensitivities involved in the IE are presented in Section 3. The proposed framework is applied in Section 4 for finding the optimal location of velocity and/or Reynolds shear stress profiles of sensors, as well as the optimal location of the sensors within the profiles, for a well-examined case of flow through a backward-facing step.

2. BAYESIAN OPTIMAL SENSOR PLACEMENT FRAMEWORK

2.1 Bayesian Parameter Estimation

The Bayesian framework for the estimation of the parameters of a CFD model based on experimental data is first outlined and the results are used for the derivation of the optimal sensor locations. Consider a CFD model and let $\underline{\theta} \in R^{N_\theta}$ be the vector of CFD model parameters to be estimated using a set of measured data $\underline{d} \equiv \underline{d}(\underline{\delta}) \in R^N$ of flow quantities at locations $\underline{\delta}$. The location vector $\underline{\delta}$ contains the coordinates of the sensors with respect to a coordinate system. Let $\underline{g}(\underline{\theta};\underline{\delta}) \in R^N$ be the vector of the values of the same flow quantities predicted by a CFD model for specific values of the parameter set $\underline{\theta}$. The following prediction error equation is introduced:

$$\underline{d} = \underline{g}(\underline{\theta};\underline{\delta}) + \underline{e} \tag{1}$$

where $\underline{e}$ is the additive prediction error term due to model and measurement error. The prediction error is modeled as a Gaussian vector, whose mean value is equal to zero and its covariance equal to $\Sigma(\underline{\sigma}) \in R^{N\times N}$, where $\underline{\sigma}$ contains the parameters that define the correlation structure of Σ. Applying the Bayesian theorem, the posterior probability density function (PDF) of $\underline{\theta}$, given the measured data $\underline{d}$, is given by

$$p(\underline{\theta}|\underline{\sigma},\underline{d},\underline{\delta}) = c\frac{1}{\left(\sqrt{2\pi}\right)^N\sqrt{\det\Sigma(\underline{\sigma})}}\exp\left[-\frac{N}{2}J(\underline{\theta};\underline{\sigma},\underline{d},\underline{\delta})\right]\pi(\underline{\theta}) \tag{2}$$

where

$$J(\underline{\theta};\underline{\sigma},\underline{d},\underline{\delta}) = \frac{1}{N}[\underline{d}-\underline{g}(\underline{\theta};\underline{\delta})]^T\Sigma^{-1}(\underline{\sigma})[\underline{d}-\underline{g}(\underline{\theta};\underline{\delta})] \tag{3}$$

expresses the deviation between the measured and model predicted quantities. The PDF $\pi(\underline{\theta})$ is the prior distribution for $\underline{\theta}$, and c is a normalization constant guaranteeing that the posterior PDF $p(\underline{\theta}|\underline{\sigma},\underline{d},\underline{\delta})$ integrates to 1.

2.2 Information Entropy—Asymptotic Approximation

The PDF $p(\underline{\theta}|\underline{\sigma},\underline{d},\underline{\delta})$, given by Eq. (2), quantifies the posterior uncertainty in the parameter values $\underline{\theta}$ based on the information contained in the measured data. The information entropy given by the expression [35]

$$h_{\underline{\theta}}(\underline{\delta};\underline{\sigma},\underline{d}) = E_{\underline{\theta}}[-\ln p(\underline{\theta}|\underline{\sigma},\underline{d},\underline{\delta})] \tag{4}$$

$$= -\int \ln p(\underline{\theta}|\underline{\sigma},\underline{d},\underline{\delta})\; p(\underline{\theta}|\underline{\sigma},\underline{d},\underline{\delta})\; d\underline{\theta} \tag{5}$$

is a scalar measure of the uncertainty of the model parameters $\underline{\theta}$. It depends on the location vector $\underline{\delta}$ of the sensors, the correlation structure of the prediction error and the details in the data $\underline{d}$.

The multi-dimensional integral in Eq. (5) is a Laplace-type integral that can be asymptotically approximated [47], for large number of data, by the expression [23]

$$h_{\underline{\theta}}(\underline{\delta};\underline{\sigma},\underline{d}) \sim H(\underline{\delta};\underline{\theta}_0,\underline{\sigma}) = \frac{1}{2}N_\theta\ln(2\pi) - \frac{1}{2}\ln\det\left[Q(\underline{\delta};\underline{\theta}_0,\underline{\sigma}) + Q_\pi(\underline{\theta}_0)\right] \tag{6}$$

where $\underline{\theta}_0$ are the values of $\underline{\theta}$ that minimize $J(\underline{\theta};\underline{\sigma},\underline{d},\underline{\delta})$; $Q(\underline{\delta};\underline{\theta},\underline{\sigma})$ is asymptotically approximated by the Fisher information matrix, a semipositive definite matrix given by [23]

$$Q(\underline{\delta};\underline{\theta},\underline{\sigma}) = \nabla_{\underline{\theta}}\underline{g}(\underline{\theta};\underline{\delta})^T \Sigma^{-1}(\underline{\sigma}) \nabla_{\underline{\theta}}\underline{g}(\underline{\theta};\underline{\delta}) \tag{7}$$

computed at the N locations where the sensors are placed; and $Q_\pi(\underline{\theta}_0) = -\nabla^T_{\underline{\theta}} \nabla_{\underline{\theta}} \ln \pi(\underline{\theta})$, evaluated at the value $\underline{\theta}_0$, with $\nabla_{\underline{\theta}} = [\partial/\partial\theta_1, ..., \partial/\partial\theta_{N_\theta}]$, represents the negative of the Hessian of the natural logarithm of the prior distribution of the model parameters.

For uniform prior distribution, the term $Q_\pi(\underline{\theta}_0) = 0$ and the optimal sensor placement are based only on the Fisher information matrix. However, for a small number of sensors, the matrix $Q(\underline{\delta};\underline{\theta},\underline{\sigma})$ can be ill-conditioned and the determinant could tend to zero independent of the location of the sensor. Such cases arise from unidentifiability issues due to the insufficient information provided by the data to estimate the number of model parameters involved. Noninformative uniform prior distributions do not provide any information to correct this problem. In has been proposed in [24] to use nonuniform distributions to remove the ill conditioning in $Q(\underline{\delta};\underline{\theta},\underline{\sigma})$ due to the extra information provided by the prior distribution about the uncertainty in the model parameters. For the specific case of a Gaussian prior distribution, the matrix $Q_\pi(\underline{\theta}_0) = \tilde{Q}$, where $\tilde{Q}$ is the inverse of the covariance matrix of the Gaussian distribution and thus it is constant independent of $\underline{\theta}$.

The asymptotic estimate (6) is very useful since it does not explicitly depend on the details of the data $\underline{d}(\underline{\delta})$, which are not available during the experimental design phase of the sensor placement. The dependence on the data comes implicitly through the optimal value $\underline{\theta}_0$ of the parameter set $\underline{\theta}$. However, since the data are not available, the optimal value $\underline{\theta}_0$ cannot be estimated. Thus optimal sensor placement designs are based on assuming a nominal value of the parameter set $\underline{\theta}_0$. Alternatively, the uncertainty in the nominal value can be accounted for as described in Section 2.3.

In addition, from Eq. (7), it can be deduced that the information entropy depends on the derivatives of the flow quantities predicted by the model at the sensor locations with respect to the model parameters. The higher the derivatives, the higher the information entropy value. The computation of these derivatives is based on the differentiation of the model with respect to the parameters, as described in Section 3.2.

2.3 Robust Information Entropy Formulation

The previous formulation is based on nominal values $\underline{\theta}_0$ assigned to the optimal value of the model parameter set $\underline{\theta}$ and the nominal values $\underline{\sigma}_0$ assigned to the prediction error parameters $\underline{\sigma}$ involved in the covariance $\Sigma(\underline{\sigma})$ of the model prediction error. A robust formulation is presented next, which takes into account the uncertainties in the augmented parameter set $\underline{\varphi}_0 = (\underline{\theta}_0, \underline{\sigma}_0)$.

Using the Bayes framework, the uncertainty in the nominal values $\underline{\varphi}_0$ of the model and prediction error parameters is quantified by the prior distribution $\pi(\underline{\varphi}_0)$. Papadimitriou et al. [22] have introduced the change of uncertainty or the change of information entropy from the prior to posterior distribution of the model parameters as a measure of the quality of a sensor configuration. The change of information entropy is given as

$$\Delta h(\underline{\delta}) = E_{\underline{\theta},\underline{\varphi}_0}[-\ln p(\underline{\theta},\underline{\varphi}_0|\underline{\delta})] - E_{\underline{\varphi}_0}[-\ln p(\underline{\varphi}_0)] \tag{8}$$

$$= \int H(\underline{\delta};\underline{\varphi}_0)\, \pi(\underline{\varphi}_0)\, d\underline{\varphi}_0 \tag{9}$$

$$= \frac{1}{2} N_\theta \ln(2\pi) - \frac{1}{2} \int \ln\det\left[Q(\underline{\delta};\underline{\varphi}_0) + Q_\pi(\underline{\varphi}_0)\right] \pi(\underline{\varphi}_0)\, d\underline{\varphi}_0 \tag{10}$$

which, using Eq. (9), is an integral of the information entropy conditioned on the nominal values of the model parameters, weighted by the prior distribution of the model parameters. The integral (9) represents the robust information entropy and arises by substituting $p(\underline{\theta},\underline{\varphi}_0|\underline{\delta}) = p(\underline{\theta}|\underline{\varphi}_0,\underline{\delta})\ \pi(\underline{\varphi}_0)$ into the definition of the information entropy given in (5) and simplifying. The equality in (10) arises after substituting the information entropy given by (6) and simplifying. Details are given in [22].

The measure (10) can be extended to include uncertainties in flow-related input quantities such as Mach number, angle of attack, and Reynolds number that are not included in the parameters to be inferred. It is straightforward to

show that the change of information entropy is given by (10), provided that the vector $\underline{\varphi}_0$ is augmented to also include these flow-related quantities. Also, it should be noted that the result (6) is a special case of (10) for the case where φ_0 is a known deterministic quantity.

Using Monte Carlo simulations or sparse grid techniques [48, 49], the integral in (10) can be approximated by

$$\int \ln\det\left[Q(\underline{\delta};\underline{\varphi}_0)+Q_\pi(\underline{\varphi}_0)\right]\pi(\underline{\varphi}_0)\,d\underline{\varphi}_0 \simeq \sum_{j=1}^{n} w_j \ln\det\left[Q(\underline{\delta};\underline{\varphi}_0^{(j)})+Q_\pi(\underline{\varphi}_0^{(j)})\right] \tag{11}$$

where $\underline{\varphi}_0^{(j)}$ are either the samples drawn from the prior $\pi(\underline{\varphi}_0)$ or the sparse grid points in the parameter space, and w_j are weights equal to $w_j = 1/n$ for the Monte Carlo technique or their values depend on the sparse grid order and the prior distribution selected [48].

2.4 Optimal Sensor Location Methodology

The sensor configuration should be designed in such a way that the measured data are as informative as possible with regard to the model parameters to be estimated. The information entropy, defined by Eq. (6), measuring the uncertainty in the parameters, gives the amount of useful information contained in the measured data. The most informative test data are those that give the least uncertainty in the parameter estimates or those that minimize the information entropy or the change of information entropy in (10). Thus the sensors should be located at the places that minimize the information entropy. It should be noted that expression (11) requires the siensitivities of the flow quantities to be computed at all sample points $\varphi_0^{(j)}$, $j = 1,\ldots,n$.

The problem of finding the optimal sensor configuration is formulated as an optimization problem where the objective function is the information entropy or the change of information entropy in the robust case and the design variables are the locations of sensors. Specifically, the optimal sensor location $\underline{\delta}_{best}$ is given by

$$\underline{\delta}_{best} = \arg\min_{\underline{\delta}} \Delta h(\underline{\delta}) \tag{12}$$

A stochastic or deterministic optimization algorithm may be used to find the location $\underline{\delta}$ of the sensors that minimizes $H(\underline{\delta};\underline{\theta}_0,\underline{\sigma})$ or $\Delta h(\underline{\delta})$. The deterministic method is usually based on the sensitivity derivatives $\partial H(\underline{\delta};\underline{\theta}_0,\underline{\sigma})/\partial\delta_i$ of the information entropy with respect to the coordinates of the sensor locations and a descent algorithm is used to locate the optimum. Although such an algorithm is quite efficient and converges very fast to the optimal solution, there is a drawback due to the several local optimals encountered in the optimal sensor location problem. Another drawback of the deterministic methods is their complexity, since the methodology to compute the aforementioned gradient components should be formulated.

In this study a stochastic optimization algorithm is employed in order to avoid the entrapment to local minima. Specifically, the covariance matrix adaptation evolution strategy (CMA-ES) [50] is used. To carry out the optimization in the continuous space of the design parameter $\underline{\delta}$, an interpolation scheme is used to compute the required values of the sensitivities involved in Eqs. (6) and (10) at locations between the grid nodes of a mesh used to discretize the spatial domain.

2.5 Prediction Error Correlation Model

In order to find the optimal location of the sensors, based on the information entropy framework, the structure of the covariance matrix $\Sigma(\underline{\sigma})$ of the prediction error correlation model should be postulated. The prediction error in (1) is due to measurement and model error. Assuming independence between the two errors, the covariance matrix takes the form $\Sigma = \bar{\Sigma} + \tilde{\Sigma}$, where $\bar{\Sigma}$ and $\tilde{\Sigma}$ are the covariance matrices of the measurement and model errors, respectively. Assuming that the measurement error is independent of the location of sensors, the covariance matrix $\bar{\Sigma}$ takes the form $\bar{\Sigma} = \bar{\sigma}^2 I$, where I is the identity matrix.

A certain degree of spatial correlation is expected for the model error, since model predictions at two neighborhood points in the physical space are usually correlated due to the structure of the model. It was demonstrated in [35] that

when the optimal sensor placement algorithm is applied on the continuous space for uncorrelated model errors, it tends to place sensors very close to each other, providing almost exactly the same information. This clustering of sensors is due to the wrong assumption of uncorrelated prediction errors and can be avoided when the correlation structure of the model predictions is taken into account. It has been theoretically shown [35] that two or more sensors within an area in the spatial domain of the size of the correlation length tend to be placed further apart in order to increase the information provided by the sensors. However, how far these sensors will be placed from each other is also controlled by the gradients of the output QoI with respect to the model parameters $\underline{\theta}$ involved in the definition of the information matrix. Very high derivatives tend to limit the size of the area affected by the correlation length. Drastic changes in the sensitivities of the QoI to parameter changes that occur between two closely spaced sensors may justify the clustering of such sensors with qualitatively distinct information [23].

A certain degree of correlation should be accounted for by the model errors between any two locations, depending on the flow physics. The correlation is postulated by selecting the correlation $\tilde{\Sigma}_{kl}$ between two sensor locations $\underline{x}_k$ and $\underline{x}_l$ in the physical space as

$$\tilde{\Sigma}_{kl} = \sqrt{\tilde{\Sigma}_{kk}\tilde{\Sigma}_{ll}}R(\eta_{kl}) \tag{13}$$

where $R(\eta_{kl})$ is the spatial correlation structure, which is assumed herein to depend on the distance $\eta_{kl} = |\underline{x}_k - \underline{x}_l|$ between the measurements k and l at locations $\underline{x}_k$ and $\underline{x}_l$, respectively. The variance $\tilde{\Sigma}_{kk}$ of the prediction error at measured location $\underline{x}_k$ can be taken to be $\tilde{\Sigma}_{kk} = \tilde{\sigma}^2 g_k^2(\underline{\theta})$ to reflect the fact that the standard deviation of the error will depend on the intensity $g_k(\underline{\theta})$ of the prediction of the output QoI in the measured location, where $\tilde{\sigma}$ is the standard deviation of the error normalized with respect to the intensity of the output QoI. For demonstration purposes, the spatial correlation structure $R(\eta_{kl})$ is selected to be of the exponential form

$$R(\eta_{kl}) = \exp\left[-\frac{\eta_{kl}}{\lambda}\right] \tag{14}$$

where λ is a measure of the spatial correlation length. Thus the parameter set $\underline{\sigma}$ involved in the covariance matrix Σ is given by $\underline{\sigma} = (\bar{\sigma}, \tilde{\sigma}, \lambda)$. The prediction error correlation model (14) has also been used in parameter estimation of the Spalart-Allmaras turbulence model [12, 18]. Other choices of correlation structures could be explored [12]. However, this falls outside the scope of the present study.

The correlation model in the prediction error dominates the information provided by two sensors within the correlation length, causing this information content to increase as a function of the distance of the sensors within the correlation length, avoiding sensor clustering [35]. In Section 4, the effect of the prediction error correlation length on the optimal location of sensors is examined, showing that small values of λ results in undesired sensor clustering, while relatively high values of λ avoids sensor clustering.

3. COMPUTATIONAL FLUID DYNAMICS MODEL

3.1 Flow Equations

The estimation of the parameters of any flow model may be conducted by the proposed methodology. Since in CFD the uncertainties in RANS turbulence model parameters are of high importance, this paper focuses on this direction and specifically, on the estimation of the Spalart-Allmaras model parameters. Thus, the flow model consists of the Reynolds-averaged Navier-Stokes equations for compressible fluid flow and the Spalart-Allmaras one-equation turbulence model. The mean-flow equations are written as

$$R_n = \frac{\partial U_n}{\partial t} + \frac{\partial f_{nk}^{inv}}{\partial x_k} - \frac{\partial f_{nk}^{vis}}{\partial x_k} = 0 \tag{15}$$

where, for steady flows, t is the pseudotime, and the conservative variables U_n and the inviscid f_{nk}^{inv} and viscous f_{nk}^{vis} fluxes are given by

$$\begin{bmatrix} U_1 \\ U_2 \\ U_3 \\ U_4 \\ U_5 \end{bmatrix} = \begin{bmatrix} \rho \\ \rho u_1 \\ \rho u_2 \\ \rho u_3 \\ E \end{bmatrix}, \quad \begin{bmatrix} f_{1k}^{inv} \\ f_{2k}^{inv} \\ f_{3k}^{inv} \\ f_{4k}^{inv} \\ f_{5k}^{inv} \end{bmatrix} = \begin{bmatrix} \rho u_k \\ \rho u_1 u_k + p\delta_{k1} \\ \rho u_2 u_k + p\delta_{k2} \\ \rho u_3 u_k + p\delta_{k3} \\ u_k(E+p) \end{bmatrix}, \quad \begin{bmatrix} f_{1k}^{vis} \\ f_{2k}^{vis} \\ f_{3k}^{vis} \\ f_{4k}^{vis} \\ f_{5k}^{vis} \end{bmatrix} = \begin{bmatrix} 0 \\ \tau_{1k} \\ \tau_{2k} \\ \tau_{3k} \\ u_m\tau_{km} + q_k \end{bmatrix} \tag{16}$$

In Eq. (16), u_k, $E = \rho e + (1/2)\rho u_k^2$, $\tau_{km} = \mu_{eff}(\partial u_k/\partial x_m + \partial u_m/\partial x_k) + \lambda\delta_{km}(\partial u_l/\partial x_l)$, and $q_k = k(\partial T/\partial x_k)$ stand for the velocity components, total energy per unit volume, viscous stresses, and heat fluxes, respectively, and $\lambda = -(2/3)\mu_{eff}$, where μ_{eff} is the sum of molecular and turbulent viscosities, μ and μ_t, respectively. Also, δ_{km} is the Kronecker symbol.

The Spalart-Allmaras model equation for compressible flows is written as follows [51]:

$$\begin{aligned} R_{\tilde{\mu}} = {} & \frac{\partial\left(\rho v_k \tilde{\mu}\right)}{\partial x_k} - \frac{1+c_{b2}}{\sigma_{SA}}\frac{\partial}{\partial x_k}\left[\left(\mu+\tilde{\mu}\right)\frac{\partial\tilde{\mu}}{\partial x_k}\right] \\ & + \frac{c_{b2}}{\sigma_{SA}}\left(\mu+\tilde{\mu}\right)\frac{\partial}{\partial x_k}\left(\frac{\partial\tilde{\mu}}{\partial x_k}\right) - \rho\tilde{\mu}P + \tilde{\mu}D = 0 \end{aligned} \tag{17}$$

where $P = c_{b1}\widetilde{S}$, $D = c_{w1}f_w(\tilde{\mu}/d^2)$ are the production and destruction terms, respectively, $\tilde{\mu}$ is the turbulence state variable, and d is the distance from the wall boundary. The turbulent viscosity coefficient μ_t is written as an expression of $\tilde{\mu}$ as follows:

$$\mu_t = \tilde{\mu} f_{v1} \tag{18}$$

Also,

$$\chi = \frac{\tilde{\mu}}{\mu}, \quad f_{v1} = \frac{\chi^3}{\chi^3 + c_{v1}^3}, \quad f_{v2} = \frac{1}{\left(1+\chi/c_{v2}\right)^3}, \quad f_{v3} = \frac{1}{\chi}\left(1+\chi f_{v1}\right)\left(1-f_{v2}\right) \tag{19}$$

and

$$\begin{aligned} & S = \sqrt{2\Omega_{ij}\Omega_{ij}}, \quad \widetilde{S} = f_{v3}S + \frac{\tilde{\mu}}{\rho\kappa^2 d^2}f_{v2} \\ & g = r + c_{w2}\left(r^6 - r\right), \quad f_w = g\left(\frac{1+c_{w3}^6}{g^6+c_{w3}^6}\right)^{1/6}, \quad r = \frac{\tilde{\mu}}{\rho\widetilde{S}\kappa^2 d^2} \end{aligned} \tag{20}$$

where $\Omega_{ij} = 1/2\left(\partial v_i/\partial x_j - \partial v_j/\partial x_i\right)$, and summation is implied for repeated indices.

The turbulence model parameters $\underline{\theta}$ to be identified are c_{b1}, c_{b2}, κ, σ, c_{w2}, c_{w3}, c_{v1}, and c_{v2}. The sensitivity of the flow variables with respect to the turbulence model parameters are derived from the differentiation of the discretized flow equations [45] in Section 3.2.

3.2 Sensitivity Analysis

In order to compute the information entropy using Eqs. (6) and (7), the sensitivities $\nabla_{\underline{\theta}}\underline{g}(\underline{\theta};\underline{\delta})$ of the output QoI $\underline{g}(\underline{\theta};\underline{\delta})$ need to be computed. For axial velocities and Reynolds shear stress sensors, the sensitivities of the axial velocities $\underline{g}^u = u_1$ and the Reynolds shear stresses $\underline{g}^s = \mu_t\left(\partial u_1/\partial x_2 + \partial u_2/\partial x_1\right)$ at each grid node with respect to the model parameters $\underline{\theta}$ are required. The sensitivities at any spatial location $\underline{\delta}$, required for the computation of the information entropy during the application of the optimization procedure, is then computed from the corresponding sensitivities at the grid cell where this location belongs using interpolation schemes.

Since the number of grid nodes that belong to the region where the sensors are to be placed is much greater than the number of model parameters, the direct differentiation approach is preferred rather than the adjoint formulation [45]. The cost of the former scales with the number of model parameters, whereas the cost of the latter scales with the number of quantities of interest, which in our case is equal to the number of grid nodes that belong to the region of interest.

The direct differentiation of the turbulence model equations has been presented in [52–54] for the k-ϵ turbulence model with wall functions, aiming at the estimation of the sensitivities of quantities of interest with respect to the turbulence model parameters. The corresponding adjoint approach to turbulence modelling has been presented in [46, 55] (discrete adjoint) and [56–58] (continuous adjoint) for the efficient optimization of turbulent flows, modelled using low Reynolds turbulence models, or high Reynolds models with wall functions.

On the other hand, a backward or forward finite difference scheme for the computation of $d\underline{g}/d\underline{\theta}$ would involve the solution of the same number of systems of equations with the direct-differentiation approach (or twice this number for central finite differences). The sensitivity values in that case would be, however, quite sensitive to the choice of $\delta\underline{\theta}$ and would not be ensured to be accurate, incorporating, also, a greater computational cost for the solution of the flow equations for the perturbed values of $\underline{\theta}$, since greater accuracy would be required.

In the direct differentiation approach, the sensitivities of the flow variables U_k with respect to the turbulence model parameters θ_i are derived from the differentiation of the discretized flow equations [45] as follows:

$$\frac{dR_n}{d\theta_i} = \frac{\partial R_n}{\partial \theta_i} + \frac{\partial R_n}{\partial U_k}\frac{dU_k}{d\theta_i} = 0 \tag{21}$$

In Eq. (21), $\partial R_n/\partial\theta_i$ are the partial sensitivities of the residual of the flow equations R_n with respect to the model parameters θ_i computed by finite differences, and $\partial R_n/\partial U_k$ is the Jacobian matrix of the flow equations residual with respect to the flow variables, computed analytically. The sensitivities of quantities g_l with respect to θ_i are computed using the chain rule as

$$\frac{dg_l}{d\theta_i} = \frac{\partial g_l}{\partial \theta_i} + \frac{\partial g_l}{\partial U_k}\frac{dU_k}{d\theta_i} \tag{22}$$

In a similar way, the sensitivities $\partial g_l/\partial\theta_i$ are the partial sensitivities of quantities g_l with respect to θ_i. In the case of $g_l = g_l^u$, these sensitivities are zero, since the velocities do not depend directly on the turbulence model parameters, which is not the case for $g_l = g_l^s$, since they are related directly to θ_i through the expression of the turbulent viscosity μ_t [Eq. (18)]. Also, $\partial g_l/\partial U_k$ is the Jacobian matrix of the derivatives of the quantities g_l with respect to the flow variables U_k.

It should be mentioned that, for $g_l = g_l^u$, the "frozen turbulence" assumption, where the sensitivity of the turbulence state variable with respect to the model parameters is neglected, cannot be used since it would lead to zero sensitivities. In the case of $g_l = g_l^s$, the computed sensitivities using the frozen turbulence assumption would not be zero but equal to $\partial g_l^s/\partial\theta_i = \partial g_l^s/\partial\theta_i$. These sensitivities, however, are still expected to be quite wrong compared to those computed using the full approach implemented in this study.

Finally, it should be made clear that the solution of the direct-differentiation equations is only made once at the initial step of the optimization algorithm, and then, an interpolation scheme is used to find the required sensitivities at each location in the flow domain.

In order to compute the information entropy, the first step is to compute the sensitivities of the flow variables with respect to the parameters at the location $\underline{\delta}$ required by the optimizer. The element in the computational mesh to which this location belongs is first found, and then the quadrilateral interpolation scheme is applied to compute the sensitivity values with respect to the sensitivities at the nodes of the grid element. In this study, an unstructured grid of quadrilateral elements is used, and thus the sensitivities $\mathrm{der}(x, y)$ at the current location (x, y) within a grid element (Fig. 1) are computed by

$$\mathrm{der}(x, y) = a + bx + cy + dxy \tag{23}$$

where the constants a, b, c, and d for each element are computed by satisfying Eq. (23) for the four element nodes as follows:

$$\mathrm{der}(x_i, y_i) = a + bx_i + cy_i + dx_iy_i,\ i = 1, ..., 4 \tag{24}$$

where the values for $\mathrm{der}(x_i, y_i)$ for $i = 1, ..., 4$ are provided by the sensitivity analysis for all nodes. The system (24) is solved for the four constants, and then the value of the sensitivity derivatives of the flow variables with respect to the model parameters at any location is computed using Eq. (23), resulting, finally, in the computation of the information entropy.

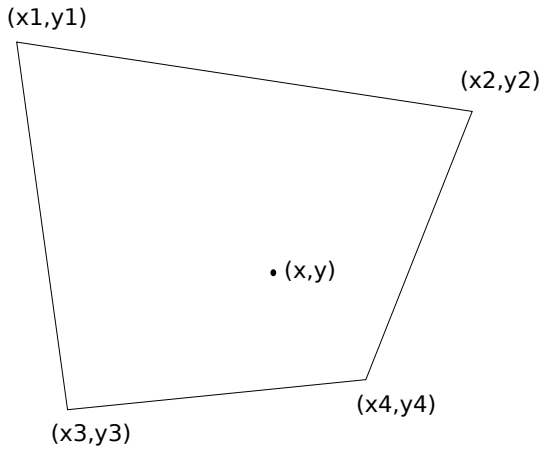

FIG. 1: Schematic view of a quadrilateral element.

It is worth pointing out that the information entropy is a continuous function of the sensor locations inside each element in the computational mesh and discontinuous along the element boundaries. The discontinuity in the element boundaries arises mainly from the spatial discretization of the flow equations, yielding discontinuous Reynolds stresses and their derivatives with respect to the model parameters. Using a stochastic optimization such as CMA-ES [50] to carry out the optimization, the search for the optimal sensor locations is not affected by such discontinuities, since the algorithm is based only on the values of the objective function and not its derivatives with respect to the sensor locations.

4. APPLICATIONS

The proposed algorithm for the optimization of the location of sensors for the estimation of parameters of CFD models is applied to the flow through a 2D backward-facing step configuration [59]. The flow domain is shown in Fig. 2. In this case, the turbulent boundary layer encounters a sudden backstep, causing flow separation. The flow then reattaches and recovers downstream of the step. The Reynolds number based on step height is equal to 36,000 and the inlet Mach number is equal to 0.128. The step height is equal to 1 m when the distance of the two walls is equal to 9 m. The velocity streamlines within the flow domain are illustrated in Fig. 3. It can be seen that the flow separates after the step and reattaches after a certain length. The flow problem, domain and computational schemes are summarized in the NASA website http://turbmodels.larc.nasa.gov/backstep_val.html.

In this work, the optimal location of profiles of velocities and Reynolds stresses are sought so that the measurements will lead to the least uncertainty in the estimates of the turbulence model parameters. A computational grid

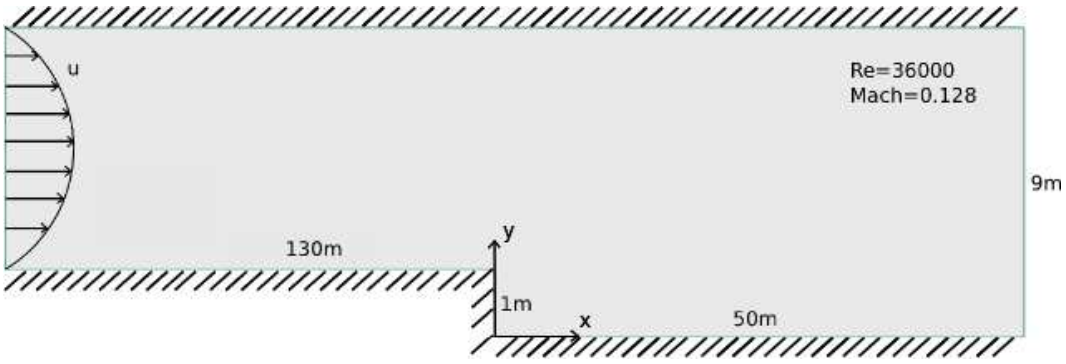

FIG. 2: Schematic view of the backward-facing step case.

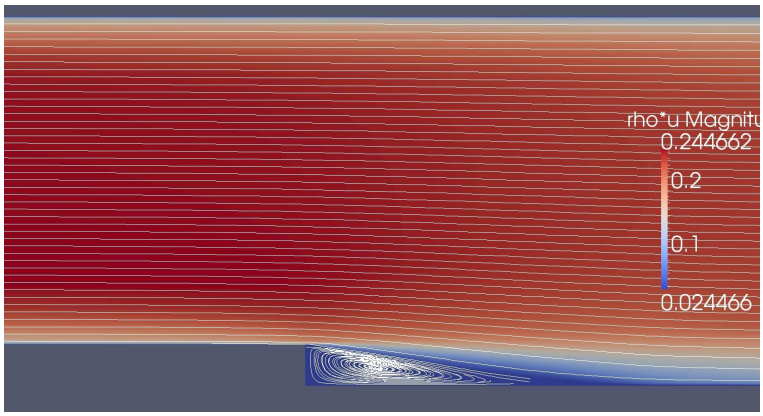

FIG. 3: Velocity streamlines and contours corresponding to the initial set of parameters.

with 4992 quadrilaterals was used to simulate the flow, obtained from the aforementioned cite of NASA. The optimal locations $\underline{\delta}$ of velocity and Reynolds stress sensors are sought that minimize the information entropy, given by Eq. (6), in the case of design based on a nominal model, or the robust information entropy, given by (10), in the case of robust design that accounts for nominal model and prediction error uncertainties.

Indicative CPU costs are given herein for the comparison of the computational cost required for each part of the sensor location optimization. The computation of the fields of the sensitivity derivatives of the measured quantities with respect to the eight Spalart-Allmaras model parameters is equal to about 2 min for each parameter at an Intel Core i7 computer at 3.7 GHz, almost equal to that of the solution of the flow equations. The prerequisite computation of the sensitivity plots is about 18 min. For robust optimization, the cost is multiplied by the number of sparse grid points n used to compute the integral (11).

Each sensor location is characterized by two design variables, the x and y coordinate of the sensor location. Three different sensor models (SM) are considered for the location of sensors:

- **Sensor model SM1**: The design variable vector is defined as $\underline{\delta} = \underline{x} = (x_1, x_2, \ldots, x_p)$, where x_i are the positions of profiles of sensors, while the positions of the sensors within each profile are predefined. The number of design variables N_d is equal to the number of profiles N_p. In the cases that follow, each profile contains five or ten sensors with predefined distances between them. The positions for five sensors are $\underline{y} = (0.2, 0.5, 1.0, 1.5, 2.0)$, while for ten sensors are $\underline{y} = (0.2, 0.4, 0.6, 0.8, 1.0, 1.2, 1.4, 1.6, 1.8, 2.0)$.

- **Sensor model SM2**: The design variable vector is defined as $\underline{\delta} = (x_1, x_2, \ldots, x_p, y_1, d)$, where x_i are the positions of profiles of sensors, y_1 is the position of the first sensor at each profile, and d is the distance between the sensors within the profile, the same for each profile. The number of design variables in this case is equal to $N_d = N_p + 2$, where N_p is the number of profiles.

- **Sensor model SM3**: The design variable vector is defined as $\underline{\delta} = (x_1, x_2, \ldots, x_p, y_1, d_2, \ldots, d_s)$, where x_i are the positions of profiles of sensors, y_1 is the position of the first sensor, and $d_i, i = 2, \ldots, N_s$ are the distances between sensors i and $i-1$, the same for each profile. The number of design variables in this case is equal to $N_d = N_p + N_s$, where N_p is the number of profiles and N_s is the number of sensors within each profile. The distances between the profiles and the sensors within the profile are not allowed to be lower than a predefined value, which is herein chosen to be equal to 0.1.

For example, if 15 sensors are used (forming three profiles) the numbers of design variables for sensor models SM1, SM2, and SM3 are equal to 3, 5, and 8, respectively. It is expected that the greater the number of design variables, the lower the optimal value of the information entropy for the same number of sensors [35] and the higher the required CPU cost for the convergence of the optimization algorithm.

The area in which the optimal locations of the sensors are sought is the orthogonal area forming a 10×2 rectangle with a height of 2 m when the step size is equal to 1 m and a length of 10 m, within which the flow is separated and reattached. The placement of a sensor above $y = 2$ m and after $x = 10$ m proved to affect the value of the information entropy quite insignificantly. Also, unless it is otherwise explicitly mentioned, the spatial correlation length in the model prediction error equation, Eq. (14), is selected to be equal to $\lambda = 0.2$ m.

The distributions of the sensitivities of the axial velocities with respect to the eight Spalart-Allmaras model parameters at the area where the separation and reattachment of the flow takes place, required to compute and optimize the information entropy, are shown in Figs. 4 and 5. It can be deduced that the axial velocity is most sensitive to the fourth turbulence model parameter c_{b1}. The second most important turbulence model parameter is κ. Also, there is some sensitivity with respect to c_{w2} and σ, while the axial velocity seems to be significantly less sensitive to the other four parameters of the Spalart-Allmaras model.

The corresponding distributions of the sensitivities of the Reynolds shear stress with respect to the eight parameters are shown in Figs. 6 and 7. As expected, the turbulence model parameters are much more informative to the Reynolds shear stress quantity, which is a quantity directly connected to the turbulence model through the turbulence viscosity. Thus, the mean sensitivity values for all parameters are greater than the values that correspond to the axial velocities. Also, the relative qualitative importance of the parameters is the same as the case of the axial velocity, with c_{b1} being again the most informative parameter.

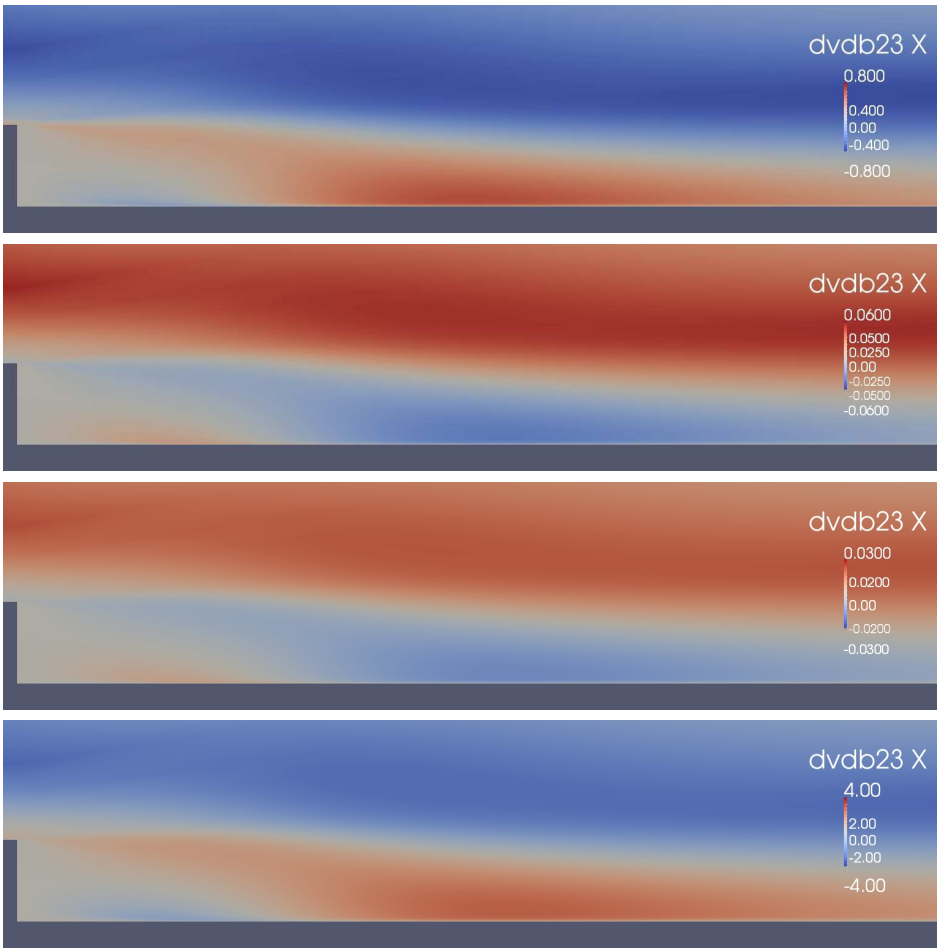

FIG. 4: Distributions of the sensitivity derivatives of the axial velocity with respect to the Spalart-Allmaras model parameters κ, c_{v1}, c_{v2}, and c_{b1}.

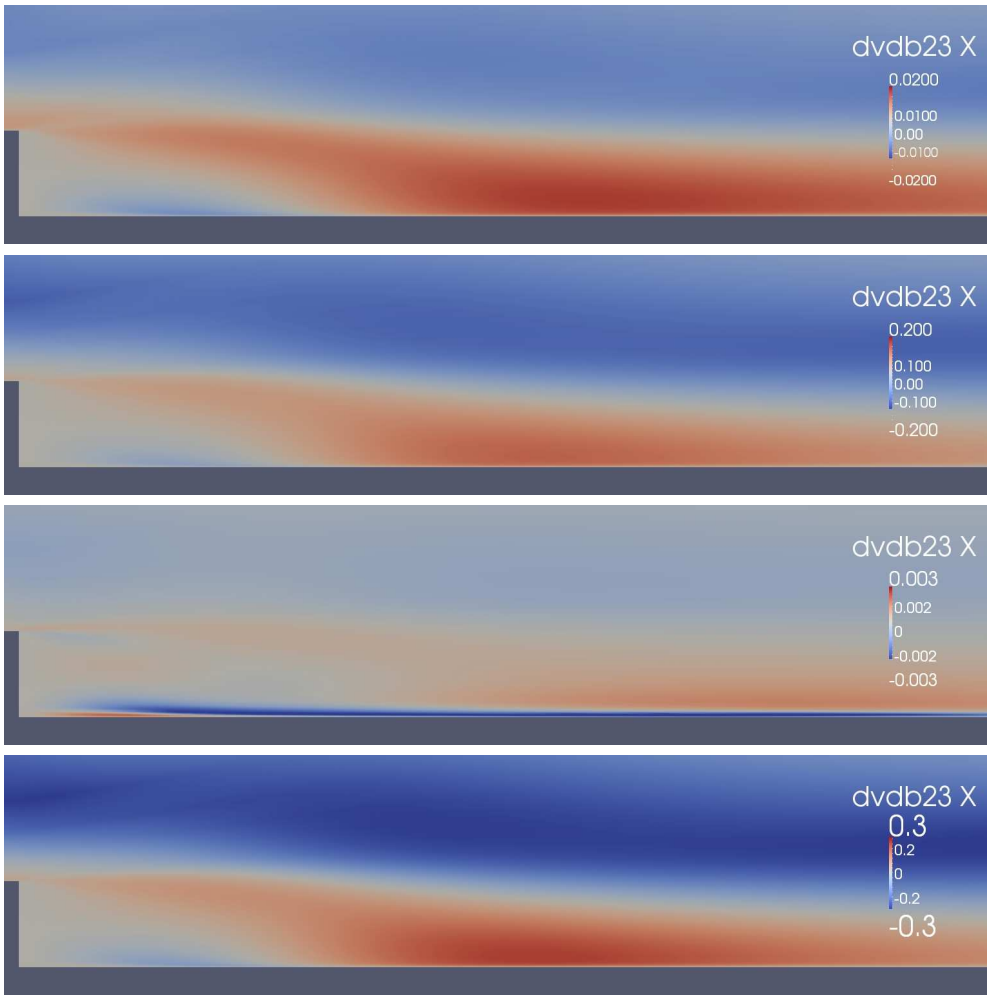

FIG. 5: Distributions of the sensitivity derivatives of the axial velocity with respect to the Spalart-Allmaras parameters c_{b2}, c_{w2}, c_{w3}, and σ.

The computations of the optimal sensor locations are based on the nominal values of the turbulence model parameters ($c_{b1}=0.1355$, $c_{b2}=0.622$, $\kappa=0.41$, $\sigma=2/3$, $c_{w2}=0.3$, $c_{w3}=2$, $c_{v1}=7.1$, and $c_{v2}=5$) given in [51]. A uniform probability density distribution of the model parameters is employed in the following demonstrations. A Gaussian distribution is also tested, offering the advantage of the elimination of the singularity of the information entropy in the case of the placement of only a few sensors. An optimal sensor configuration design based on the robust measure (10) is also used to take into account the uncertainties in the nominal model parameter values by considering that uncertainties follow a Gaussian distribution, with mean value equal to the nominal value and standard deviation equal to 10% of the mean values. The experimental error is assumed to follow a Gaussian distribution, with zero mean and standard deviation equal to $\bar{\sigma} = 0.03\%$. The model error is assumed Gaussian as well, with zero mean and standard deviation proportional to the velocity or Reynolds stress and equal to $\tilde{\sigma} = 20\%$ of their local value.

First, the optimal location of one profile of five velocity sensors is investigated for the case of uniform prior distribution using the sensor model SM1. Since this problem has only one design variable, the dependence of the information entropy on the profile location can be shown explicitly. Figure 8(left) gives the information entropy (6) as a function of the profile location based on the nominal values of the model parameters. The global optimal location is found to be $x = 1.20$, corresponding to a value of information entropy equal to $h = 7.84$. The condition number of Q

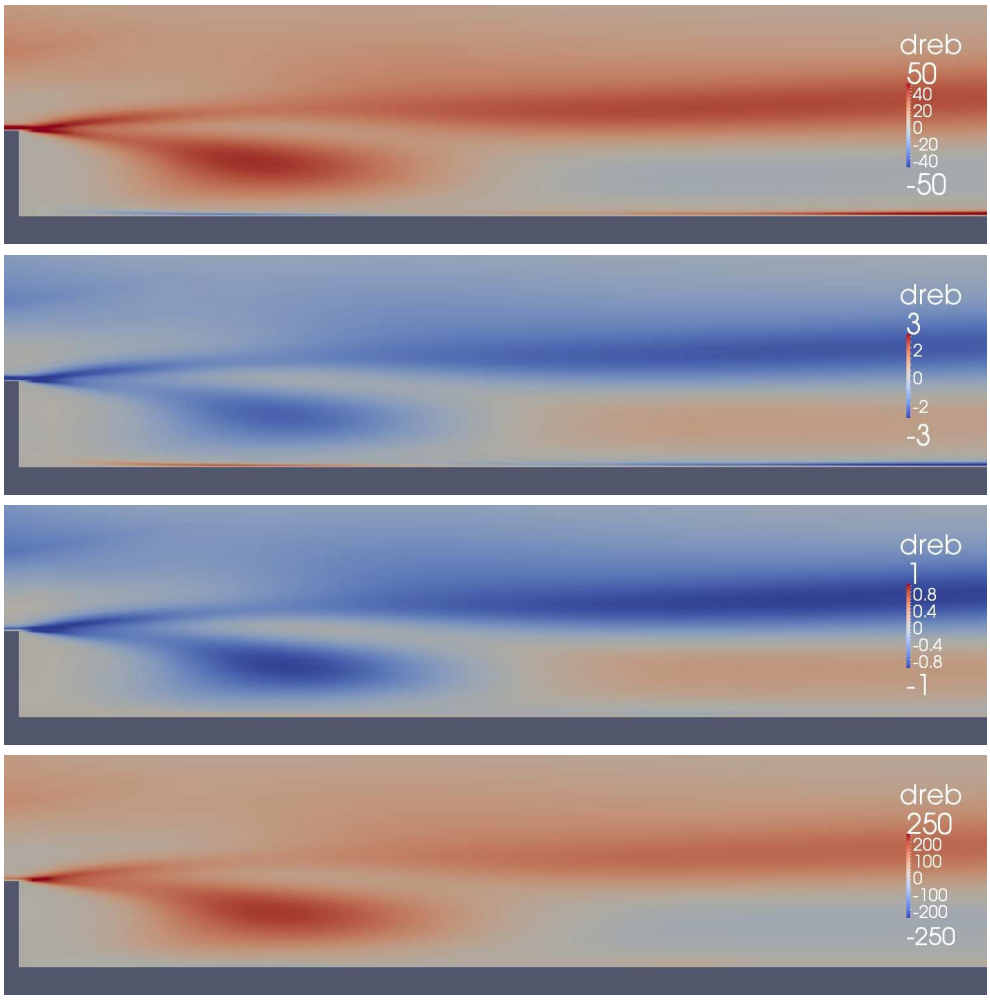

FIG. 6: Distributions of the sensitivity derivatives of the Reynolds stresses with respect to the Spalart-Allmaras parameters κ, c_{v1}, c_{v2}, and c_{b1}.

in this case was above 10^{20}, revealing that the five sensors on a single profile are insufficient for the estimation of the values of all eight parameters. For such unidentifiable cases, the information entropy tends to infinity, independently of the location of the sensor profile. The information entropy in the unidentifiable cases is computed using (6) with $\log[\det(Q + Q_\pi)] = \log[\det Q] = \sum_{k=1}^{m_c} \lambda_k$, where λ_k, $k = 1, \ldots, m_c$ are the eigenvalues of the matrix Q and m_c is the number of eigenvalues whose values are higher than a prespecified value, usually selected to be a small fraction of the maximum eigenvalue. The information entropy, in Fig. 8(left) was computed by omitting the three smaller eigenvalues whose values were lower than 10^{-10}. A local optimum is also found in Fig. 8(left) at $x = 3.52$ with the information entropy being equal to $h = 8.26$. In the case of one Reynolds shear stress profile (with five sensors), the minimum value for the information entropy is found for $x = 0$ due to the high sensitivities of the Reynolds stresses with respect to the turbulence model parameters observed at $x = 0$ (see Figs. 6 and 7). There are also some local minima, as shown in Fig. 8(right).

In the case of a Gaussian prior distribution of the model parameters, the information entropy values (6) and the robust information entropy values (10) as a function of the sensor profile location are compared in Fig. 9(left) and 9(right) for velocity and Reynolds stress measurements, respectively. Comparing the information entropy results corresponding to the nominal model parameter values in Figs. 8(left) and 9(left) for the uniform and Gaussian prior,

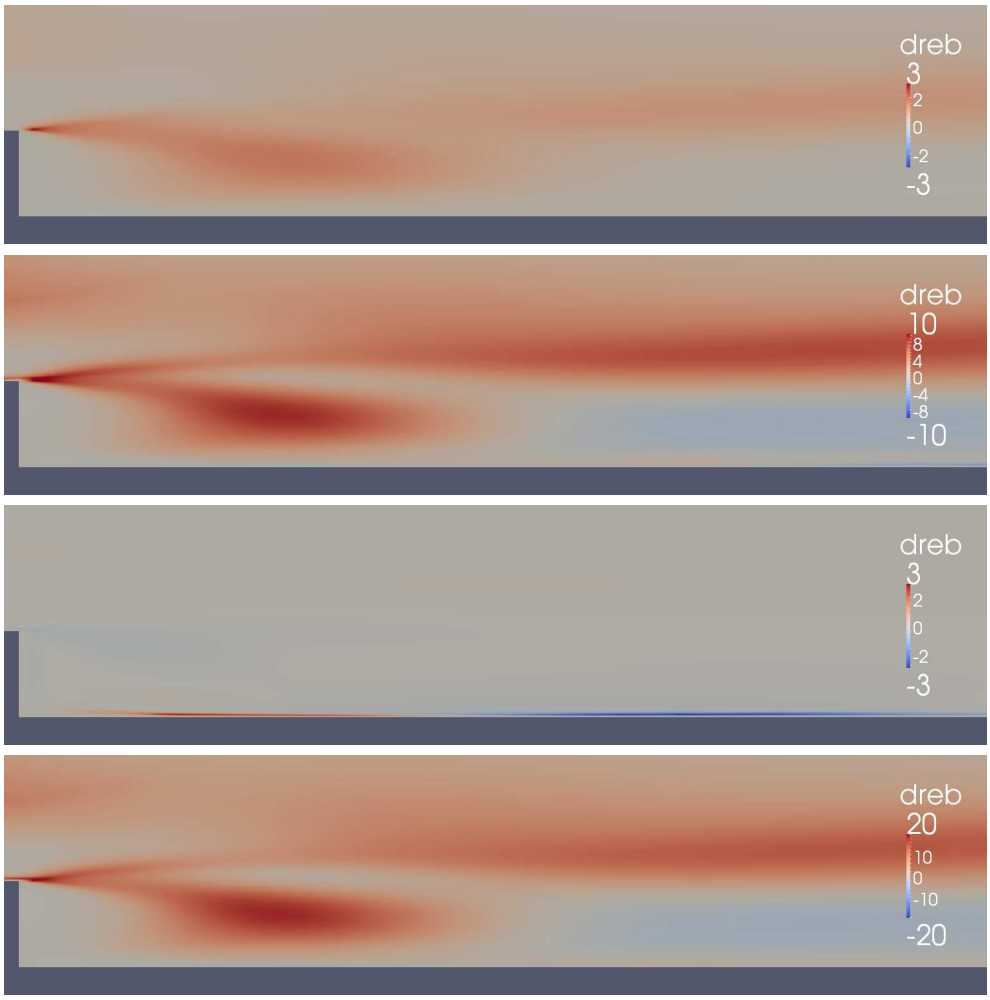

FIG. 7: Distributions of the sensitivity derivatives of the Reynolds stresses with respect to the Spalart-Allmaras parameters c_{b2}, c_{w2}, c_{w3}, and σ.

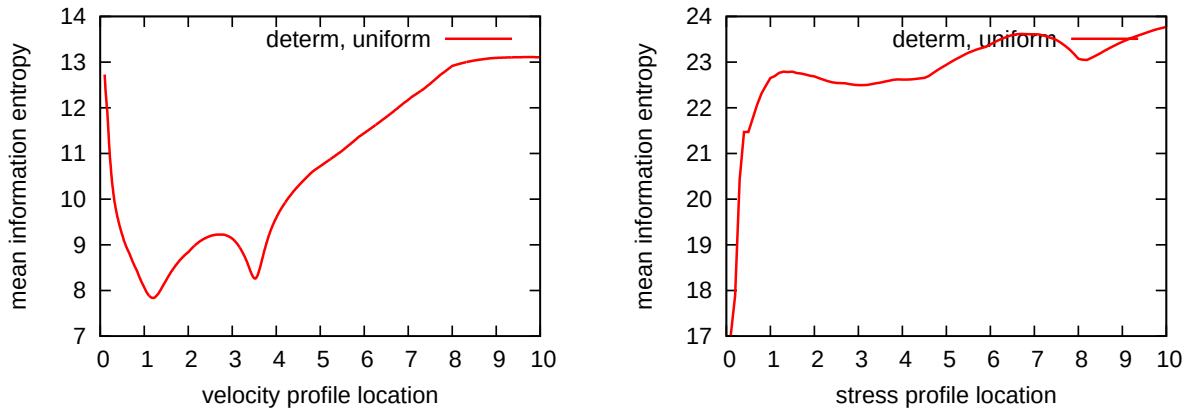

FIG. 8: Information entropy value with respect to the location of one velocity profile (left) or one Reynolds stress profile (right) for the case of a uniform prior PDF.

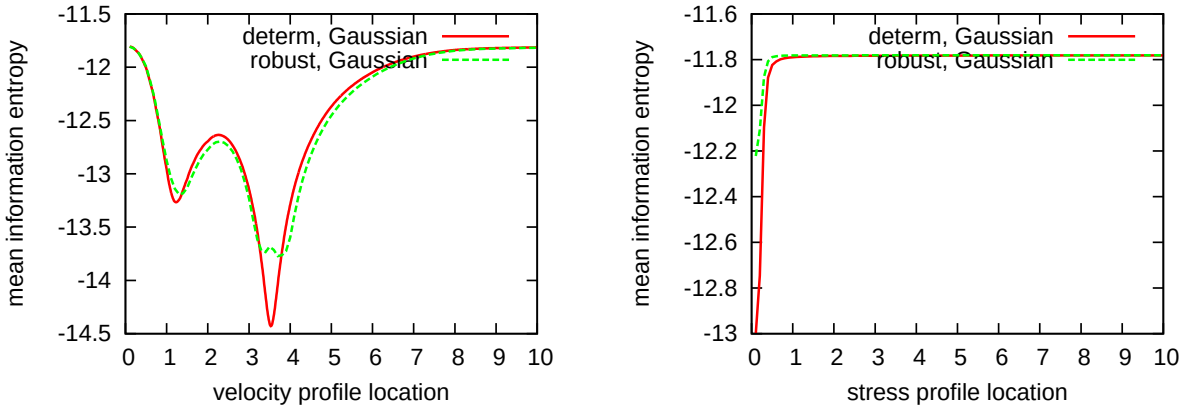

FIG. 9: Information entropy and robust information entropy value with respect to the location of one velocity profile (left) or one Reynolds stress profile (right) for the case of a Gaussian prior PDF.

respectively, it is evident that there is a switch between the global and the local optimum in the case of velocity measurements. The optimal profile location for the Gaussian prior is at $x = 3.52$ instead of $x = 1.20$ for the uniform prior distribution. The robust optimal sensor location is affected only slightly by the uncertainties in the nominal values of the turbulence model parameters, moving the optimal position of the profile slightly to the right of $x = 3.52$.

It should be noted that for each location of the sensor profile, the robust result is an average of the neighborhood information entropy values. As a result, the robust information entropy values close to the deterministic optimal are always higher than the minimum value of the information entropy obtained for the nominal values of the model parameters. This explains the smallest information entropy value obtained at $x = 3.52$ in Fig. 9(left) for the deterministic case, with the magnitude of the difference between the optimal robust information entropy value and the optimal information entropy value for the deterministic case to depend on the level of parameter uncertainty considered. From the results in Fig. 9(right), similar observations are in effect about the variation of the robust information entropy and the nominal information entropy values with respect to the Reynolds stress sensor profile location. The optimal sensor profile is placed at $x = 0$ for the robust design as well.

In the case of more than one profile, there are several local optima in the problem and thus a gradient-based optimization algorithm is not suitable for finding the global optimum. For this reason, the CMA-ES algorithm [50] was employed to solve the optimal sensor location problem. The correlation length in these cases is very important in order to avoid the clustering of the profiles. The influence of the correlation length λ is illustrated in Fig. 10 for

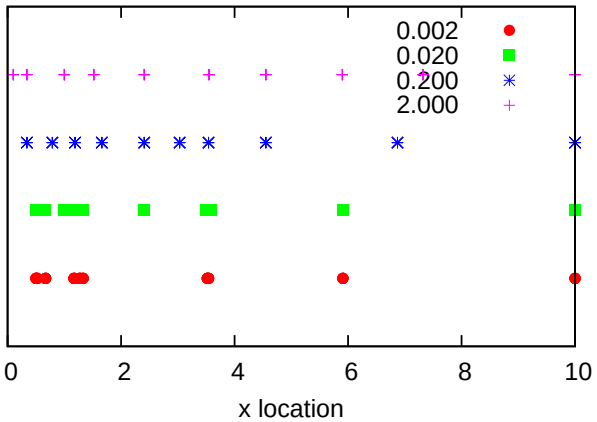

FIG. 10: Optimal location of six velocity profiles using four different values of correlation length λ.

the sensor model SM1 for ten velocity profiles. It can be seen that the profiles are allowed to be clustered in the cases of $\lambda = 0.002$ and $\lambda = 0.02$, while if the value of λ is higher, the sensors tend to be more scattered, avoiding clustering.

Indicative results of optimal locations of one to ten velocity profiles and the corresponding information entropy values are shown in Fig. 11 for correlation length $\lambda = 0.2$ and for the nominal values of the turbulence model parameters. In these cases, the uniform prior distribution of the model parameters was employed, since no singularities appear in the case of more than one profile. The optimal sensor locations are estimated for the nominal values of the turbulence model parameters. The information entropy in Fig. 11(right) is compared also to the case that the profile has ten predefined sensors instead of five and to the minimum possible information entropy, obtained by placing a large number of 50 profiles with 5 or 10 sensors with equal distances between them. The case that the locations of the profiles are not optimized but are equally spaced along the direction x is also included in this figure. It can be seen that the optimal location of the first profile is at $x = 1.20$ and the optimal location of the second profile is at $x = 3.52$, where the global and local optima of the 1D problem were located. If three profiles are to be used, it is recommended that the profiles are located at $x = 1.02$, $x = 2.41$, and $x = 3.56$. As the number of profiles increases, the profiles are located between $x = 0$ and $x = 7$, and only after the seventh profile placement is a profile located at the end of the domain.

The information entropy [Fig. 11(right)] decreases as the number of sensors increases. There is a sharp drop of the information entropy for a low number of sensors placed at their optimal location, and for large numbers of sensors the rate of decrease of the information entropy is significantly smaller. Thus the optimal placement of more than a number of profiles of sensors is not expected to contribute significantly to the quality of the obtained information. Also, the cases of ten sensors per profile seem to provide slightly more information (corresponding to smaller information entropy values) for more than two profiles since, for example, three, four, and five profiles of ten sensors yield slightly less information entropy values than the ones corresponding to six, eight, and ten profiles of five sensors. For one and two profiles of ten sensors each, the information entropy is higher than the one obtained for two and four profiles of five sensors each. Thus, given a fixed number of sensors, for a low number of profiles it is best to use fewer of sensors, say five instead of ten, per optimally placed profile. For a larger number of profiles, the opposite is true, i.e., it is best to use more sensors per profile.

In Fig. 12, the optimal location of one to ten Reynolds shear stress profiles is shown. The optimal location of the first profile is close to the step while the optimal location of the second profile is at $x = 4$. The additional profiles have to be placed so that they cover three subregions, one close to the step from $x = 0$ to $x = 1$, another one between $x = 2$ and $x = 5$, and the third one between $x = 7$ and $x = 10$. Due to the imposition of the spatial correlation length, no pair of sensors is found to be placed too close with each other. The information entropy is decreasing quite a lot

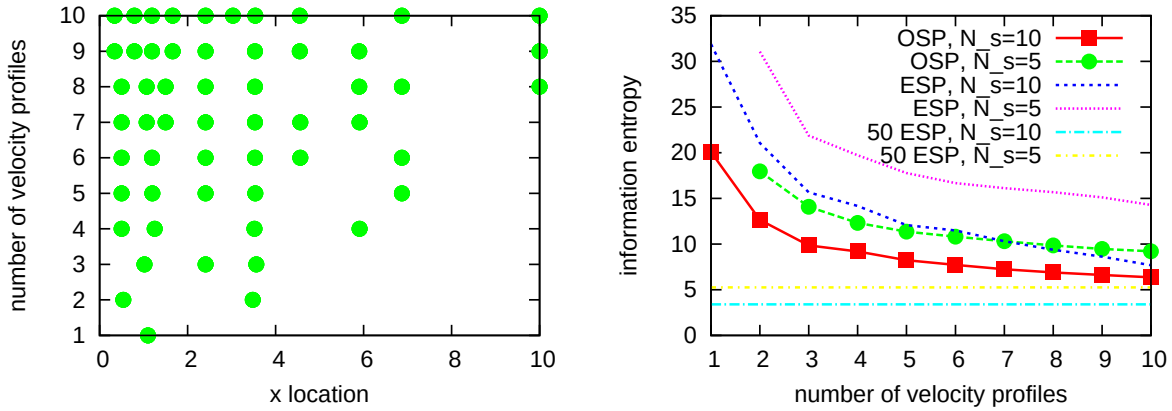

FIG. 11: Optimal location of one to ten velocity profiles of five sensors (left). Minimum information entropy values (right) as a function of number of profiles for five and ten sensors per profile, along with information entropy values for one to ten and a large number of 50 equally spaced profiles. OSP and ESP stand for "optimally spaced profiles" and "equally spaced profiles", respectively.

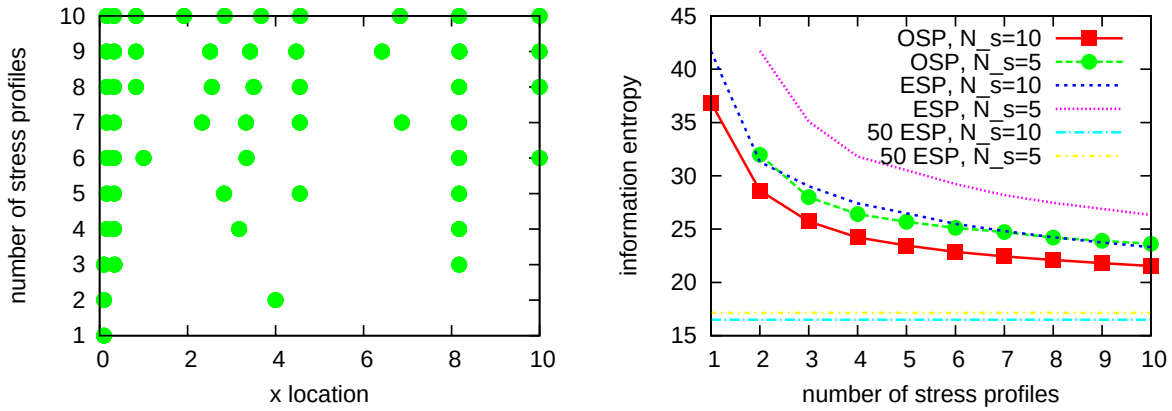

FIG. 12: Optimal location of one to ten Reynolds stress profiles of five sensors (left). Minimum information entropy values (right) as a function of number of profiles for five and ten sensors per profile, along with information entropy values for one to ten and a large number of 50 equally spaced profiles. OSP and ESP stand for "optimally spaced profiles" and "equally spaced profiles", respectively.

upon the placement of the second and third profile, and the decrease rate is not significant from the fourth to the tenth profile.

Furthermore, it should be mentioned that the optimization of the location of velocity and Reynolds stress sensors seems to be quite important, since the difference with information entropy values of the nonoptimized configurations observed in Figs. 11(right) and 12(right) is quite noticeable.

The simultaneous optimization of velocity and Reynolds stress profiles is shown in Fig. 13 for all the combinations of one to five velocity profiles with one to five Reynolds stress profiles. The top-left subfigure corresponds to one velocity profile and one up to five stress profiles, the second subfigure corresponds to two velocity profiles and one up to five stress profiles, and so forth. The bottom-right figure shows the minimum information entropy as a function of velocity and stress profiles. The profiles of the same type of sensors are not clustered due to the correlation length assumed for the prediction error model; however, a velocity profile may be placed close to a stress profile, since no correlation model is imposed between them. For more than two Reynolds stress profiles, two profiles are placed close to the step at $x = 0$, where separation occurs and the sensitivities are high. However, the distance between these two closely space profiles is controlled by the assumed correlation length of $\lambda = 0.2$.

The optimal locations of Reynolds stress sensors for the three sensor models SM1, SM2, and SM3 are shown in Fig. 14 for the case of two to seven profiles of five sensors each. In all cases, there is a tendency to place one or more profiles and sensors at the region close to the step where the separation starts and the sensitivities have high values. This tendency is stronger as the number of profiles increases. The comparison of the information entropy for the three sensor models corresponding to Fig. 14 is shown in Fig. 15. In all cases, the information entropy of the SM2 model is less than that corresponding to the SM1 model, and the information entropy of the SM3 model is even lower. This is due to the fact that the SM2 sensor model is more flexible than the SM1 sensor model to spread the sensors in the flow domain and collect more information. Similarly, the SM3 sensor model is more flexible than SM1 and SM2. For the SM3 case, two to three sensor profiles are located close to the step at $x = 0$ and $y = 1$, due to the high sensitivities of the Reynolds stresses with respect to the turbulence model parameters in this area of the flow domain. In general, the sensor domain is affected by the sensor model used and its flexibility to spread sensors around the flow domain. Specifically, with a small number of additional degrees of freedom (SM1: N_p, SM2: N_p+2, SM3: $N_p+N_s = N_p+5$) the measurements become more informative. It is worth noting from the results in Fig. 15 that three sensor profiles of the sensor model SM3 are more informative than five sensor profiles of SM2 or seven sensor profiles of SM1, placed at their optimal positions.

The application of the robust optimal sensor location is depicted in Fig. 16 for the case of five profiles of five Reynolds stress sensors for the three sensor models. The robust information entropy is minimized in this case. Results

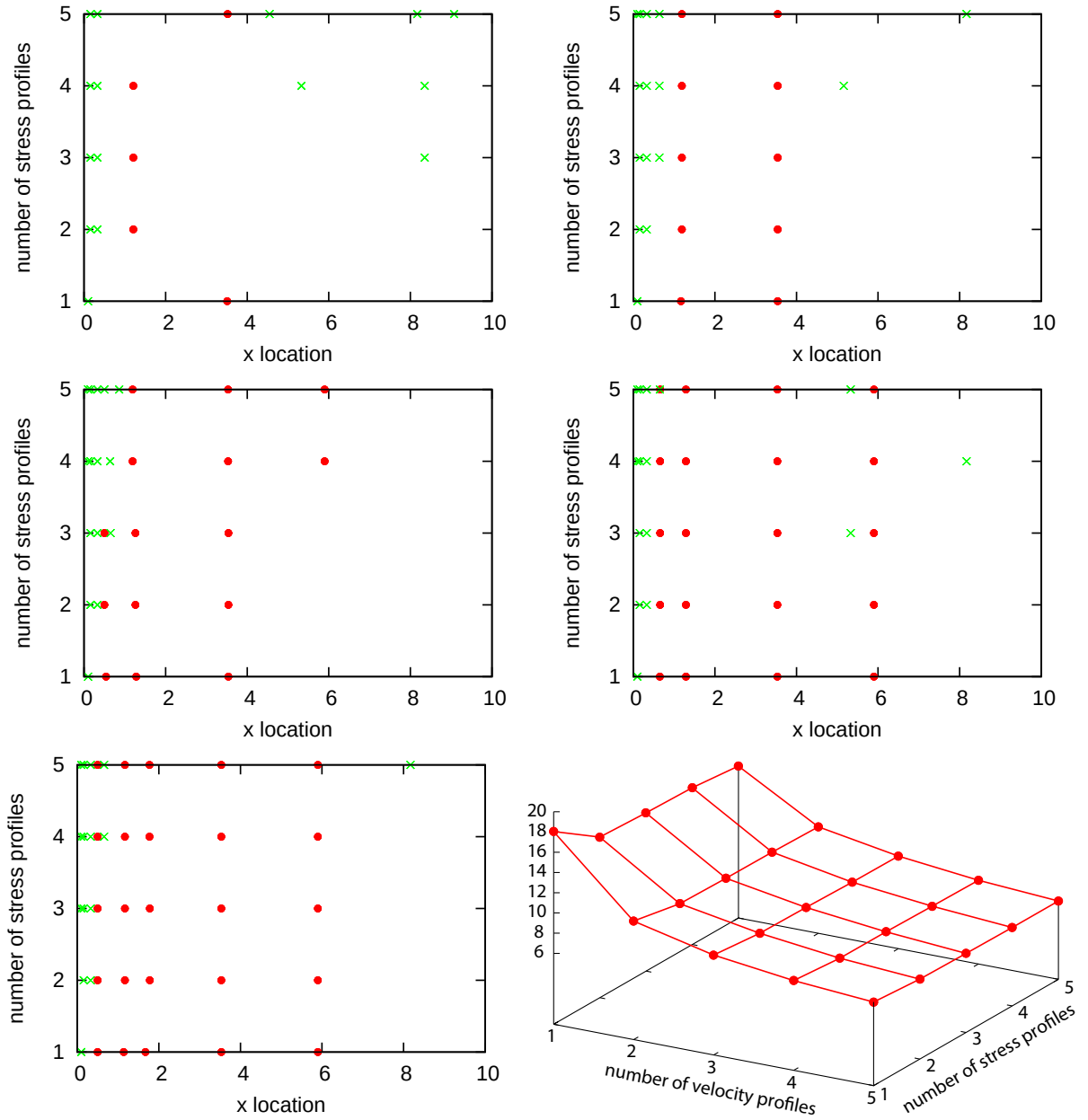

FIG. 13: Optimal location of one to five velocity (circles) and Reynolds stress profiles (crosses) of five sensors and corresponding information entropy values.

are compared to the optimal sensor locations obtained using the nominal model parameter values. It can be seen that inclusion of uncertainties led to a different location for some of the profiles for all sensor models and different locations of the sensors within the profiles.

A general remark is that several sensors are placed close to the separation region, where the gradient values are high. Also, in the case of SM1, two of the five profiles with predefined sensor locations are placed very close to the step at $x = 0$, both in the nominal case where and in the case the uncertainties are taken into account. The optimal location of a third profile is found to be close to $x = 8.1$, while the remaining two profiles are spread at intermediate

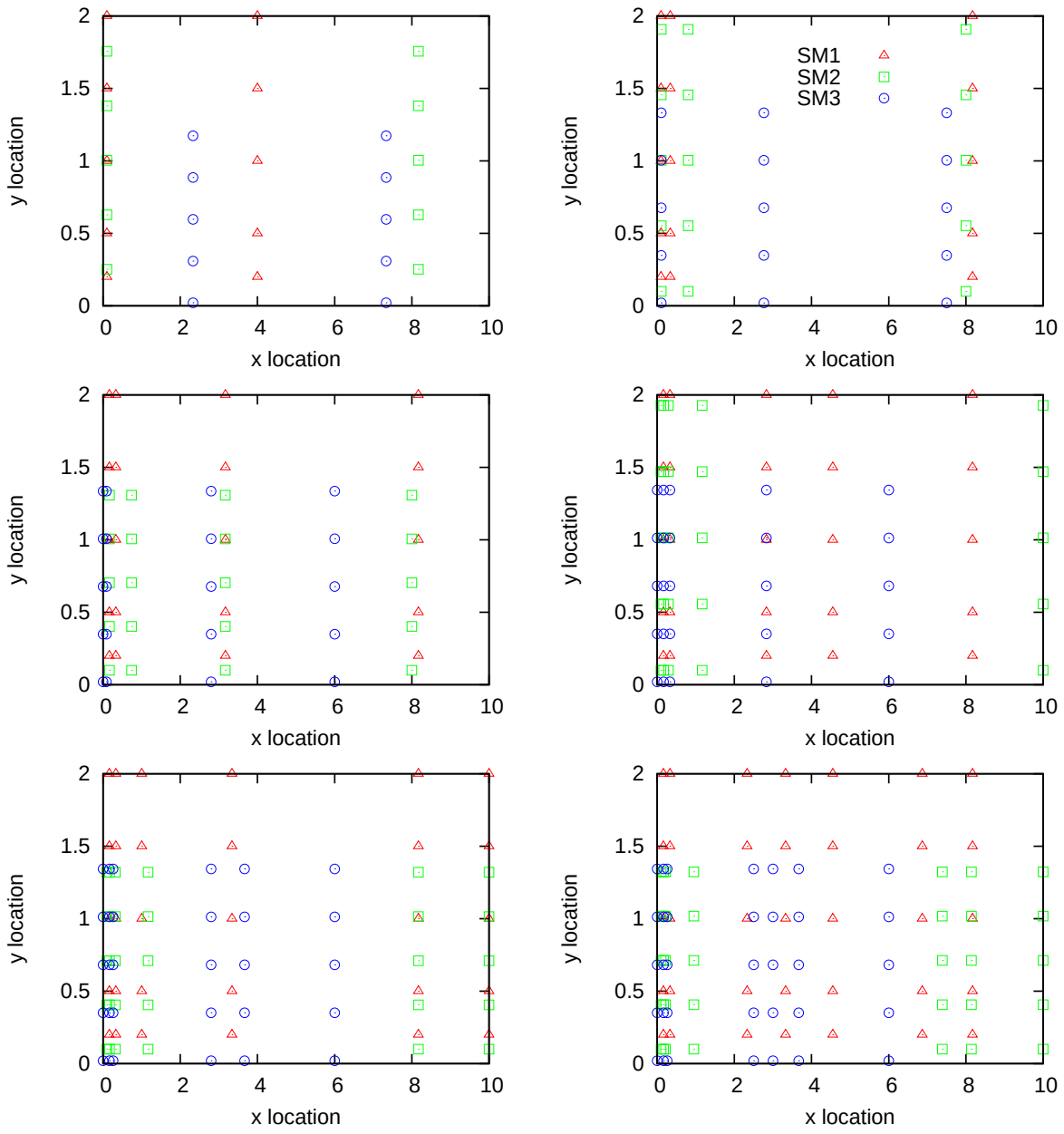

FIG. 14: Optimal location of two to seven Reynolds stress profiles with five sensors using the three different sensor models.

positions between $x = 0$ and $x = 8.1$. In the case of SM2 using the nominal values of the parameters, the first three profiles are located very close to the step and the sensors within the profile are located from $y = 0.1$ up to $y = 1.9$, in such a way that the third sensor is placed at $y = 1$ next to the step, where the gradient values are high. If the uncertainties in the model parameters are included, two of the profiles are placed close to the step in such a way that the fourth sensor is at $y = 1$. The upper last sensor in the profile is chosen to be located at $y = 1.3$, while the region above $y = 1.3$ is free of sensors. In the case of SM3 this tendency is amplified; for the nominal parameter values, three profiles are still close to the step and the fourth sensor within a profile is located at $y = 1$ while the fifth sensor

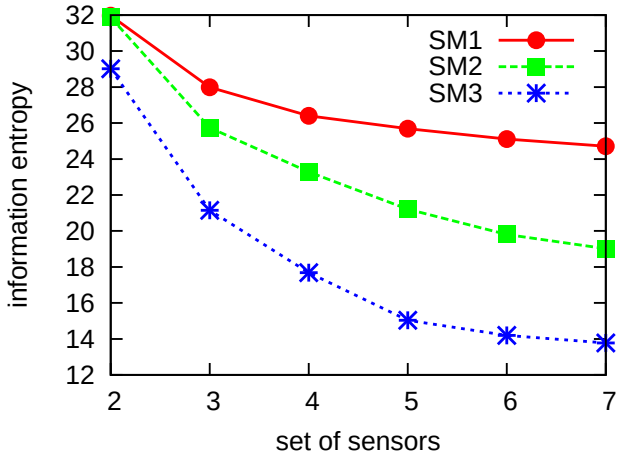

FIG. 15: Information entropy for the case of two to seven Reynolds stress profiles with five sensors using the three different sensor models.

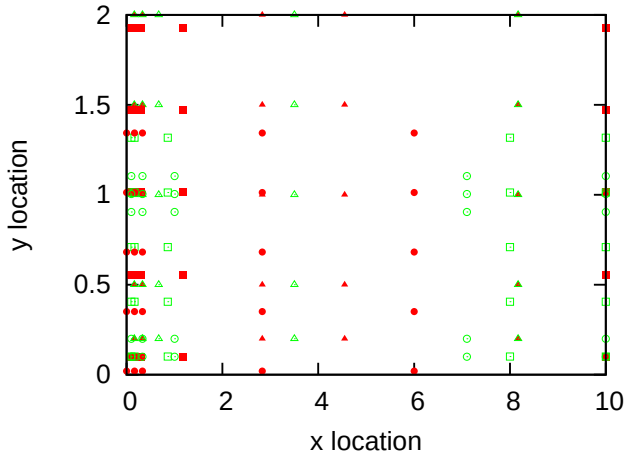

FIG. 16: Optimal location of five Reynolds stress profiles with five sensors computed based on the nominal (solid triangle, rectangle and circle) and robust (empty triangle, rectangle and circle) information entropy for the three different sensor models SM1 (triangle), SM2 (rectangle), and SM3 (circle).

is located at $y = 1.3$. The inclusion of uncertainties results in the location of three sensors around $y = 1$ and the other two around $y = 0.2$. The region above $y = 1.1$ is sensor free. Also, both for SM2 and SM3, if the uncertainties are taken into consideration, the optimal locations of profiles tend to be spread downstream of the backstep flow, covering more space.

5. CONCLUSIONS

The IE is a rational measure of the Bayesian posterior uncertainty of the CFD model parameters suitable to be used for quantifying the information contained in the data collected from a sensor configuration. Minimizing the IE with respect to the sensor positions provides the least uncertainty in the posterior parameter estimates and thus the optimal sensor configuration with the highest information. The design variables associated with the location of sensors in the flow domains of CFD problems are defined in a continuous space. The stochastic optimization algorithm CMA-ES is suitable to carry out the minimization of the IE and obtain the global optimum, avoiding premature convergence

to several observed local optima. An asymptotic estimate expresses the IE in terms of the sensitivities of the output quantities of interest with respect to the model parameters to be inferred. To avoid information redundancy that arises from sensor clustering, a spatially correlated prediction error model was used. The optimal experimental design is conditioned on nominal CFD and prediction error model parameters. To account for uncertainties in the nominal values of these model parameters and cover a number of experimental flow conditions (e.g., Mach number, angle of attack, Reynolds number), the robust information entropy is introduced as an integral of the conditional information entropy on these nominal values, weighted by the prior distribution of these parameters postulated in Bayesian analysis.

The IE framework was applied to the flow through a backward-facing step for the estimation of the Spalart-Allmaras turbulence model parameters using axial velocity and/or Reynolds shear stress profiles of sensors. The sensitivities of the velocities and Reynolds shear stresses were computed using the direct differentiation method for all grid points involved in the sparse grid approximation of the robust information entropy. The most informative sensor locations were identified for three sensor profile models. The existence of multiple local optima was clearly demonstrated, necessitating the need of using CMA-ES to perform the optimization over the continuous space. The necessity of using a spatially correlated prediction error model in order to avoid redundant information from sensor clustering was demonstrated. Systematic studies were performed to demonstrate the effect of the sensor profile models, the number and type of sensors within a profile, and the number of profiles on the information gained from optimal placement of sensors. The importance of optimizing the sensor placement, as well as choosing the optimal number of sensors within a profile, was clearly demonstrated. Reynolds stress sensor profiles were found to be more informative than the velocity sensor profiles for estimating the turbulence model parameters. More flexible sensor profile models when optimized contain more useful information for parameter estimation. The largest information gain is obtained for a relatively small number of optimally placed sensor profiles. As the number of sensor profiles increases, the information gain from extra sensor profiles reduces. The optimal number of sensor profiles to be used in an experiment is a trade-off between information gain and cost of instrumentation. Furthermore, uncertainties in the nominal model parameters are important because they lead to different sensor profile locations than the ones corresponding to the nominal parameter values. The proposed OSP framework is flexible to handle different spatially correlated modeling errors and is applicable to more general flows and turbulence models.

ACKNOWLEDGMENTS

This research project is implemented within the framework of the Action “Supporting Postdoctoral Researchers” of the Operational Program “Education and Lifelong Learning” (Actions Beneficiary: General Secretariat for Research and Technology), and is cofinanced by the European Social Fund (ESF) and the Greek State.

REFERENCES

1. Hadjidoukas, P. E., Angelikopoulos, P., Papadimitriou, C., and Koumoutsakos, P., Pi4U: A high performance computing framework for Bayesian uncertainty quantification of complex models, *J. Comput. Phys.*, 284:1–21, 2015.
2. Papadimitriou, C. and Katafygiotis, L. S., A Bayesian methodology for structural integrity and reliability assessment, *Int. J. Adv. Manuf. Syst.*, 4(1):93–100, 2001.
3. Beck, J. L., Bayesian system identification based on probability logic, *Struct. Control Health Monitoring*, 17(7):825–847, 2010.
4. Yuen, K. V., *Bayesian Methods for Structural Dynamics and Civil Engineering*, John Wiley and Sons, New York, 2010.
5. Beck, J. L. and Katafygiotis, L. S., Updating models and their uncertainties. I: Bayesian statistical framework, *J. Eng. Mech., ASCE*, 124(4):455–461, 1998.
6. Angelikopoulos, P., Papadimitriou, C., and Koumoutsakos, P., Bayesian uncertainty quantification and propagation in molecular dynamics simulations: A high performance computing framework, *J. Chem. Phys.*, 137(14):144103, 2012.

7. Angelikopoulos, P., Papadimitriou, C., and Koumoutsakos, P., *Bayesian Uncertainty Quantification And Propagation In Molecular Dynamics Simulations*, ECCOMAS, Vienna, Austria, 2012.
8. Farrell, K., Oden, J. T., and Faghihi, D., A Bayesian framework for adaptive selection, calibration, and validation of coarse-grained models of atomistic systems, *J. Comput. Phys.*, 295:189–208, 2015.
9. Wang, J. and Zabaras, N., A Bayesian inference approach to the inverse heat conduction problem, *Int. J. Heat Mass Transfer*, 47:3927–3941, 2004.
10. Jategaonkar, R., Fischenberg, D., and Gruenhagen, W., Aerodynamic modeling and system identification from flight datarecent applications at DLR, *J. Aircraft*, 41(4):681–691, 2004.
11. Oden, J. T., Hawkins, A., and Prudhomme, S., General diffuse interface theories and an approach to predictive tumor growth modeling, *Math. Models Method Appl. Sci.*, 20(3):477–517, 2010.
12. Cheung, S. H., Oliver, T. A., Prudencio, E. E., Prudhomme, S., and Moser, R. D., Bayesian uncertainty analysis with applications to turbulence modeling, *Reliab. Eng. Syst. Safety*, 96:1137–1149, 2011.
13. Oliver, T. A. and Moser, R. D., Bayesian uncertainty quantification applied to RANS turbulence models, *J. Phys. Conf. Ser.*, 318:042032, 2011.
14. Edeling, W. N., Cinnella, P., Dwight, R. P., and Bijl, H., Bayesian estimates of parameter variability in the k-ε turbulence model, *J. Comput. Phys.*, 258:73–94, 2014.
15. Kennedy, M. C. and O'Hagan, A., Bayesian calibration of computer models, *J. Royal Stat. Soc. Ser. B*, 63(3):425–464, 2001.
16. Merle, X. and Cinnella, P., Bayesian quantification of thermodynamic uncertainties in dense gas flows, *Reliab. Eng. Syst. Safety*, 134:305–323, 2015.
17. Edeling, W. N., Cinnella, P., and Dwight, R. P., Predictive RANS simulations via Bayesian modelscenario averaging, *J. Comput. Phys.*, 275:65–91, 2014.
18. Papadimitriou, D. I. and Papadimitriou, C., Bayesian uncertainty quantification of turbulence models based on highorder adjoint, *Comput. Fluids*, 120:82–97, 2015.
19. Shah, P. and Udwadia, F. E., A methodology for optimal sensor locations for identification of dynamic systems, *J. Appl. Mech.*, 45:188–196, 1978.
20. Udwadia, F. E., Methodology for optimal sensor locations for parameter identification in dynamic systems, *J. Eng. Mech.*, 120(2):368–390, 1994.
21. Qureshi, Z. H., Ng, T. S., and Goodwin, G. C., Optimum experimental design for identification of distributed parameter systems, *Int. J. Control*, 31:21–29, 1980.
22. Papadimitriou, C., Beck, J. L., and Au, S. K., Entropy-based optimal sensor location for structural model updating, *J. Vib. Control*, 6(5):781–800, 2000.
23. Papadimitriou, C., Optimal sensor placement methodology for parametric identification of structural systems, *J. Sound Vib.*, 278(4):923–947, 2004.
24. Yuen, K.-V. and Kuok, S.-C., Efficient Bayesian sensor placement algorithm for structural identification: A general approach for multi-type sensory systems, *Earthquake Eng. Struct. Dyn.*, 44(5):757–774, 2015.
25. Kripakaran, P. I. and Smith, F. C., Configuring and enhancing measurement systems for damage identification, *Adv. Eng. Inf.*, 23(4):424–432, 2009.
26. Metallidis, P., Verros, G., Natsiavas, S., and Papadimitriou, C., Identification, fault detection and optimal sensor location, *J. Vib. Control*, 9(3-4):337–359, 2003.
27. Green, P. L., Cross, E. J., and Worden, K., Bayesian system identification of dynamical systems using highly informative training data, *Mech. Syst. Signal Process.*, 56-57:109–122, 2015.
28. Robert-Nicoud, Y., Raphael, B., and Smith, I. F. C., Configuration of measurement systems using Shannons entropy function, *Comput. Struct.*, 83(8):599–612, 2005.
29. Papadopoulou, M., Raphael, B., Smith, I. F. C., and Sekhar, C., Hierarchical sensor placement using joint entropy and the effect of modeling error, *Entropy*, 16:5078–5101, 2014.
30. Bedrossian, H. and Masri, S. F., Optimal placement of sensors and shakers for modal identification, in *Computational Stochas-*

tic Mechanics, Spanos, P. D. and Deodatis, G. (Eds.), Millpress, Rotterdam, p. 5357, 2003.

31. Yao, L., Sethares, W. A., and Kammer, D. C., Sensor placement for on orbit modal identification via a genetic algorithm, *AIAA J.*, 31:1167–1169, 1993.
32. Worden, K. and Burrows, A. P., Optimal sensor placement for fault detection, *Eng. Struct.*, 23:885–901, 2001.
33. Papadopoulou, M., Raphael, B., Smith, I., and Sekhar, C., Optimal sensor placement for timedependent systems: Application to wind studies around buildings, *J. Comput. Civil Eng.*, 04015024, 10.1061/(ASCE)CP.1943-5487.0000497, 2015.
34. Kammer, D. C., Sensor placements for on orbit modal identification and correlation of large space structures, *J. Guidance Control Dyn.*, 14:251–259, 1991.
35. Papadimitriou, C. and Lombaert, G., The effect of prediction error correlation on optimal sensor placement in structural dynamics, *Mech. Syst. Signal Process.*, 28:105–127, 2012.
36. Patan, M. and Ucinski, D., Optimal location of sensors for parameter estimation of static distributed systems, *Parallel Process. Appl. Math., Lect. Notes Comput. Sci.*, 2328:729–737, 2006.
37. Stephan, C., Sensor placement for modal identification, *Mech. Syst. Signal Process*., 27:461–470, 2012.
38. Alana, J. E., Optimal measurement locations for parameter estimation of nonlinear distributed parameter systems, *Braz. J. Chem. Eng.*, 27(4):627–642, 2010.
39. Alana, J. E. and Theodoropoulos, C., Optimal location of measurements for parameter estimation of distributed parameter systems, *Comput. Chem. Eng.*, 35:106–120, 2012.
40. Morelli, E. A., Real-time aerodynamic parameter estimation without air flow angle measurements, AIAA Paper no. 2010–7951, 2010.
41. Metropolis, N., Rosenbluth, A. W., Rosenbluth, M. N., Teller, A. H., and Teller, E., Equation of state calculations by fast computing machines, *J. Chem. Phys.*, 21(6):1087–1092, 1953.
42. Beck, J. L. and Au, S. K., Bayesian updating of structural models and reliability using Markov chain Monte Carlo simulation, *ASCE J. Eng. Mech.*, 128(4):380–391, 2002.
43. Ching, J. and Chen, Y. C., Transitional Markov Chain Monte Carlo method for Bayesian updating, model class selection, and model averaging, *ASCE J. Eng. Mech.*, 133:816–832, 2007.
44. Cheung, S. H. and Beck, J. L., Bayesian model updating using hybrid Monte Carlo simulation with application to structural dynamic models with many uncertain parameters, *ASCE J. Eng. Mech.*, 135(4):243–255, 2009.
45. Papadimitriou, D. I. and Giannakoglou, K. C., Aerodynamic shape optimization using first and second order adjoint and direct approaches, *Arch. Comput. Methods Eng.*, 15(4):447–488, 2008.
46. Zervogiannis, T., Papadimitriou, D. I., and Giannakoglou, K. C., Total pressure losses minimization in turbomachinery cascades using the exact Hessian, *J. Comput. Methods Appl. Mech. Eng.*, 199:2697–2708, 2010.
47. Bleistein, N. and Handelsman, R., *Asymptotic Expansions for Integrals*, Dover Publishing Co., New York, 1986.
48. Gerstner, T. and Griebel, M., Numerical integration using sparse grids, *Numer. Algorithms*, 18:209–232, 1998.
49. Bungartz, H. J. and Griebel, M., Sparse grids, *Acta Numer.*, 13:147–269, 2004.
50. Hansen, N., Muller, S. D., and Koumoutsakos, P., Reducing the time complexity of the derandomized evolution strategy with covariance matrix adaptation (CMA-ES), *Evol. Comput.*, 11(1):1–18, 2003.
51. Spalart, P. and Allmaras, S., A one-equation turbulence model for aerodynamic flows, AIAA Paper no. 92–0439, 1992.
52. Turgeon, E., Pelletier, D., Borggaard, J., and Etienne, S., Application of a sensitivity equation method to the k-ε model of turbulence, *Optim. Eng.*, 8:341–372, 2007.
53. Caro, R., Hay, A., Etienne, S., and Pelletier, D., Application of a shape sensitivity equation method to turbulent flow over obstacles, AIAA Paper no. 2007–4207, 2007.
54. Colin, E., Etienne, S., Pelletier, D., and Borggaard, J., Application of a sensitivity equation method to turbulent flows with heat transfer, *Int. J. Thermal Sci.*, 44:1024–1038, 2005.
55. Lee, B. J. and Kim, C., Automated design methodology of turbulent internal flow using discrete adjoint formulation, *Aerospace Sci. Technol.*, 11:163–173, 2007.

56. Zymaris, A. S., Papadimitriou, D. I., Giannakoglou, K. C., and Othmer, C., Continuous adjoint approach to the Spalart-Allmaras turbulence model for incompressible flows, *Comput. Fluids*, 38:1528–1538, 2009.

57. Bueno-Orovio, A., Castro, C., Palacios, F., and Zuazua, E., Continuous adjoint approach for the Spalart-Allmaras model in aerodynamic optimization, *AIAA J.*, 50:631–646, 2012.

58. Zymaris, A. S., Papadimitriou, D. I., Giannakoglou, K. C., and Othmer, C., Adjoint wall functions: A new concept for use in aerodynamic shape optimization, *J. Comput. Phys.*, 229:5228–5245, 2010.

59. Driver, D. M. and Seegmiller, H. L., Features of reattaching turbulent shear layer in divergent channel flow, *AIAA J.*, 23(2):163–171, 1985.